Mon. Not. R. Astron. Soc. **344,** L43–L47 (2003)

A deep *Chandra* observation of the Perseus cluster: shocks and ripples

A. C. Fabian,[1⋆] J. S. Sanders,[1] S. W. Allen,[1] C. S. Crawford,[1] K. Iwasawa,[1] R. M. Johnstone,[1] R. W. Schmidt[1,2] and G. B. Taylor[3]

[1]*Institute of Astronomy, Madingley Road, Cambridge CB3 0HA*
[2]*Institut für Physik, Universität Potsdam, Am Neuen Palais 10, 14469 Potsdam, Germany*
[3]*National Radio Astronomy Observatory, Socorro, NM 87801, USA*

Accepted 2003 June 9. Received 2003 June 9; in original form 2003 April 16

ABSTRACT

We present preliminary results from a deep observation lasting almost 200 ks of the centre of the Perseus cluster of galaxies around NGC 1275. The X-ray surface brightness of the intracluster gas beyond the inner 20 kpc, which contains the inner radio bubbles, is very smooth apart from some low-amplitude quasi-periodic ripples. A clear density jump at a radius of 24 kpc to the north-east, about 10 kpc out from the bubble rim, appears to be due to a weak shock driven by the northern radio bubble. A similar front may exist around both inner bubbles but is masked elsewhere by rim emission from bright cooler gas. The continuous blowing of bubbles by the central radio source, leading to the propagation of weak shocks and viscously dissipating sound waves seen as the observed fronts and ripples, gives a rate of working which balances the radiative cooling within the inner 50 kpc of the cluster core.

Key words: shock waves – galaxies: clusters: individual: Perseus – cooling flows – intergalactic medium – X-rays: galaxies: clusters.

1 INTRODUCTION

The Perseus cluster, A426, is the X-ray-brightest cluster of galaxies in the sky. The giant central galaxy, NGC 1275, hosts the radio source 3C 84 (Pedlar et al. 1990), from which jets have blown two diametrically opposed bubbles in the hot intracluster medium (Böhringer et al. 1993; Fabian et al. 2000). Surrounding NGC 1275 is a spectacular Hα nebulosity with filaments extending over 100 kpc (Lynds 1970; Conselice, Gallagher & Wyse 2001).

The radiative cooling time of the hot gas drops inward to $\sim 10^8$ yr around NGC 1275, and the temperature drops down from $\sim$7 to about 3 keV. As has been found for many clusters with *Chandra* and *XMM–Newton* data (Peterson et al. 2001, 2003; Tamura et al. 2001), there is little gas at lower temperatures. A standard cooling flow (Fabian 1994) is not taking place despite the short cooling times, presumably because of some balancing heat source. Plausible heat sources are an active galactic nucleus (Tucker & Rosner 1983; Tabor & Binney 1993; Churazov et al. 2000; Böhringer et al. 2002) and the hot atmosphere surrounding the active galactic nucleus (AGN) (Bertschinger & Meiksin 1986; Narayan & Medvedev 2001). The jets and bubbles may heat the surrounding gas from the centre (Brüggen & Kaiser 2001; Quilis, Bower & Balogh 2001; Reynolds, Heinz & Begelman 2001; Basson & Alexander 2003) or thermal conduction may heat it from the outside (Voigt et al. 2002; Fabian, Voigt & Morris 2002c; Zakamska & Narayan 2003). Combinations of heating and conduction have also been proposed (Ruszkowski & Begelman 2002). It has proven difficult in many models to match the observed temperature profiles (Brighenti & Mathews 2003). Other possibilities involving inhomogeneous metallicity (Fabian et al. 2001; Morris & Fabian 2003) and mixing with cooler gas (Fabian et al. 2001, 2002b) remain.

We observed the core of the Perseus cluster with *Chandra* for about 25 ks in 2001 (Fabian et al. 2000; Schmidt, Fabian & Sanders 2002). Here we report on a recent *Chandra* observation which was almost 10 times deeper ($\sim$200 ks). The complex two-dimensional temperature distribution of the hot gas is now clear, and subtle structures are revealed. These may be dissipating sound waves caused by the bubbles. The power from the sound waves is consistent with the radiative losses of the cluster core.

The Perseus cluster is at a redshift of 0.0183. We assume that $H_0 = 70$ km s^{-1} Mpc^{-1} so that 1 kpc corresponds to about 2.7 arcsec.

2 ANALYSIS

Two observations of the cluster were made using *Chandra* with its ACIS-S detector, on 2002 August 8 (exposure 95.8 ks) and 10 (exposure 95.4 ks). The data sets show no evidence for contamination by flares, and were merged into a single events file since the nominal roll angle of the spacecraft was essentially identical. The analysis presented here was made on this merged events file, which was processed with the acisD2000-08-12gainN0003 gain file.

The spectral analysis was made on the data from the S3 chip, although the neighbouring chips were used for imaging. The data

⋆E-mail: acf@ast.cam.ac.uk

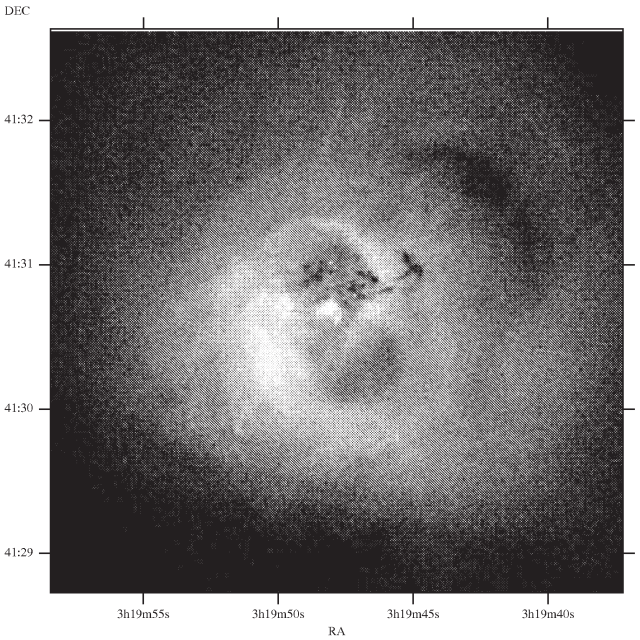

Figure 1. Central regions of the cluster in the 0.3–1.5 keV band. Pixels are 0.49 arcsec in dimension. North is to the top of this image. Absorption from the 8000 km s^{-1} system projected to the north of the nucleus of NGC 1275 is evident, as are wisps to the north and north-west which correlate with optical Hα filaments.

sets were processed using CIAO 2.3, and XSPEC 11.2 was used to analyse the spectra.

We show in Fig. 1 an image of the 0.3–1.5 keV emission from the central ∼5.5 arcmin with 0.49-arcsec pixels. The image was corrected for two linear nodal structures (at position angle 80° near the top and the lower third of the image), by dividing by an exposure map generated using the CIAO MERGE_ALL script. Similar images in the 1.5–3.5 and 3.5–7 keV bands are shown in Fig. 2, binned on 0.98- and 1.96-arcsec pixels respectively. The radio bubbles are surrounded by a ∼10 kpc thick region of hard X-ray emission (see Fig. 2, lower panel) and by structured softer patches and rims (see Figs 1 and 7).

To reveal the larger scale structure in the cluster we used unsharp masking. A 0.3–7 keV exposure-map-corrected image was smoothed with Gaussians of fixed width 0.98 and 9.8 arcsec; the two smoothed images were then subtracted, the result of which is shown in Fig. 3. Areas in which there was a deficit of counts relative to the larger scale are shown as black, and areas that showed a surplus are shaded white. It can be seen that there are a number of ripple-like structures which lie outside the outer radio lobes. We have investigated a range of smoothing lengths; the smaller one must be less than a few arcsec and the larger one about half a ripple wavelength. When their location is known, the ripples can be discerned by eye in the original raw image. The implication of the ripples is discussed in a later section.

To quantify the level of these fluctuations in the unsmoothed image, we generated a radial profile between PA 300° and 320°, across the north-west outer radio lobe. The flux per pixel in 0.98 arcsec wide annuli is shown in Fig. 4. Between these angles, the positive maxima (relative to the local mean) of the fluctuations are at radii of ∼115 and ∼135 arcsec. We also show the profile to the north-east, across the interesting, sharp-edged, emission region just outside the rim of the inner northern bubble. Its edge, or front, is at a radius of about 60 arcsec.

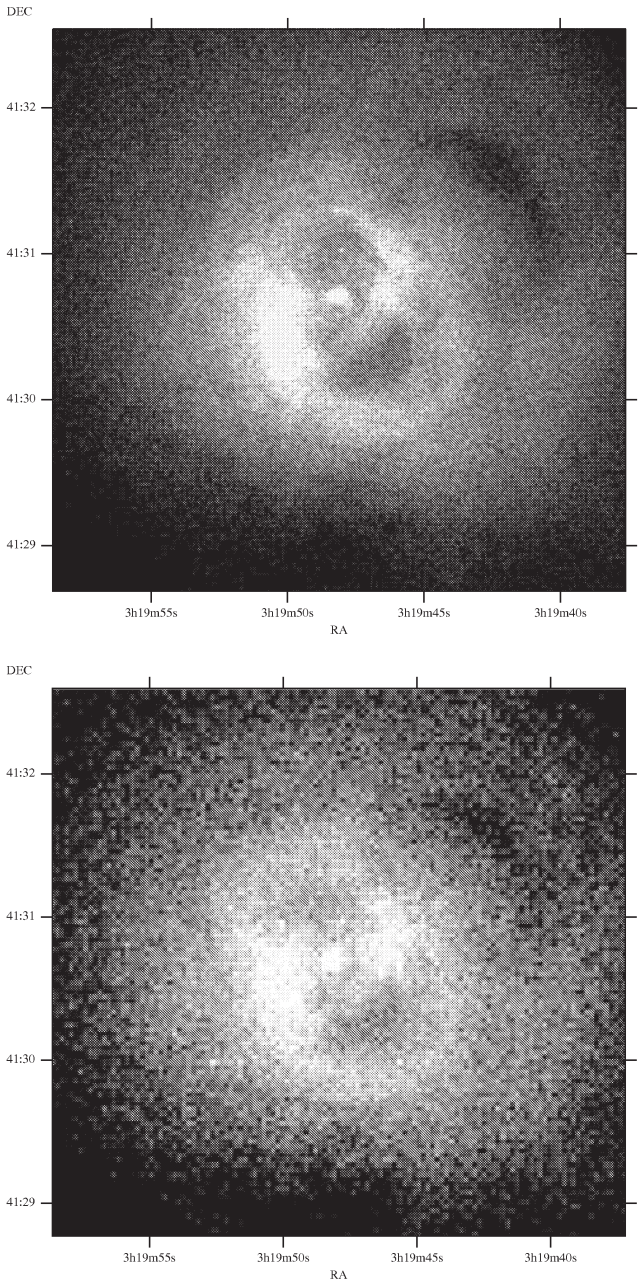

Figure 2. Images in the 1.5–3.5 (upper) and 3.5–7 keV (lower) bands, binned on 2 and 4 raw pixels, respectively.

In Fig. 5 (opposite p. L52) we show contours from a 328-MHz Very Large Array (VLA) image. This image has been made from combining VLA observations taken in the A, B and C configurations to produce an image with 8-arcsec resolution and good sensitivity to extended emission. To produce the deprojected X-ray image, the average contribution to the emission from outer shells was subtracted from the pixels within a pixel-width shell, assuming spherical symmetry around the central source. This procedure highlights non-radial features in the intensity map.

To create a temperature map of the cluster, we extracted spectra from regions containing ∼2000 counts between 0.5 and 7 keV (signal-to-noise ratio ∼45), produced using the bin-accretion algorithm of Cappellari & Copin (2003). The spectra were binned to contain at least 20 counts per spectral bin. The ∼6500 spectra were

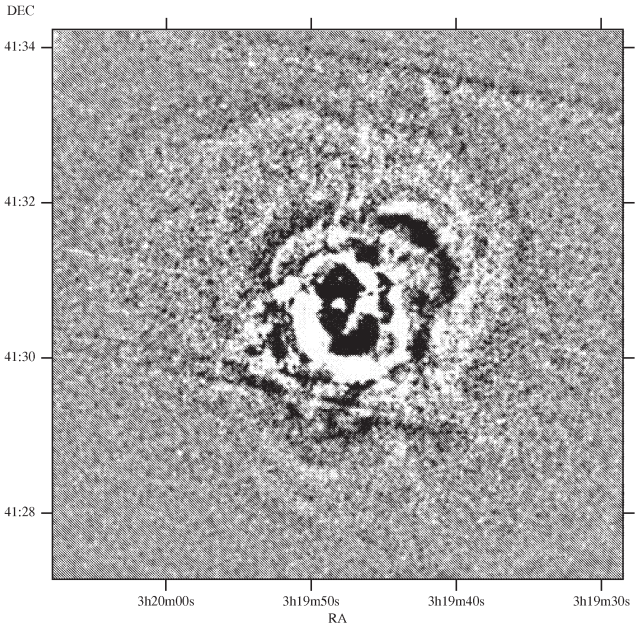

Figure 3. Unsharp-masked image created by smoothing a 0.3–7 keV intensity image by a $\sigma = 9.8$ arcsec Gaussian, subtracting the original image, then smoothing by a 0.98-arcsec Gaussian. The nodal lines in the detector, mentioned in the text, can be seen running across the image.

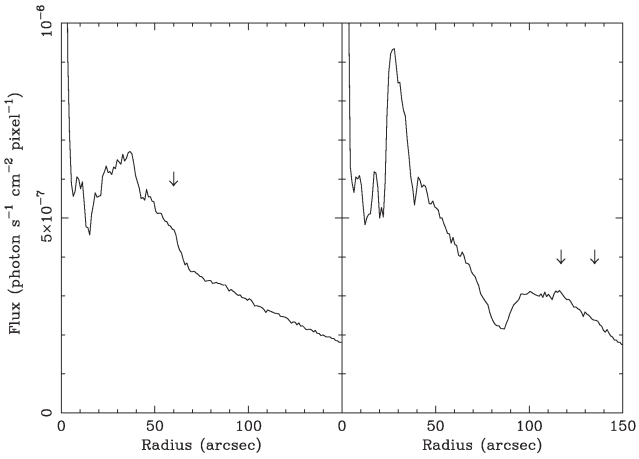

Figure 4. Radial profile in the 0.3–7 keV band between PA (left) 14°–60° and (right) 300°–320°. Arrows indicate the front (left panel) and ripples (right-hand panel). Flux uncertainties due to Poisson noise are 1–2 per cent.

then fitted between 0.5 and 7 keV with a MEKAL spectral model (Mewe, Gronenschild & van den Oord 1985; Liedahl, Osterheld & Goldstein 1995) absorbed by a PHABS model (Balucinska-Church & McCammon 1992). When fitting the spectra, the temperature, abundance (assuming ratios of Anders & Grevesse 1989) and column density were allowed to be free. Ancillary-response matrices and response matrices were made using the CIAO MKWARF and MKRMF programs, weighting the responses to regions based on the number of counts between 0.4 and 7 keV. The ancillary-response matrix was then corrected using the CORRARF routine to correct for the ACIS low-energy degradation,[1] applying the ACISABS absorption profile of Chartas & Getman (2002). When fitting, we used a background

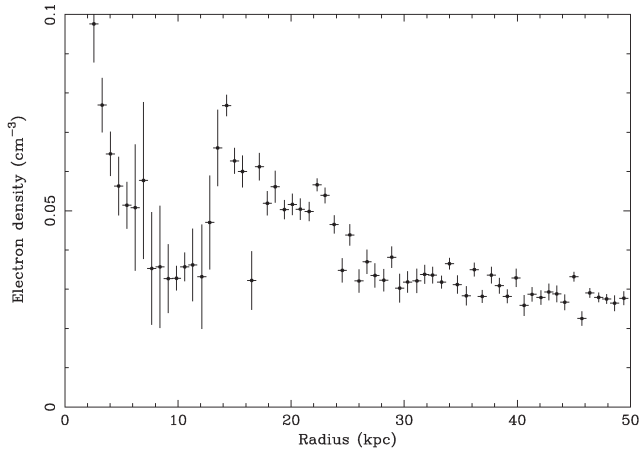

Figure 8. Deprojected density profile in a sector to the north-west (PA = 14°–60°).

spectrum generated from a blank-sky observation in CALDB for this period of observation.

Finally, we made a temperature map (Fig. 6, opposite p. L52) by smoothing the best-fitting temperatures (accurate to around 10 per cent, providing the spectral model is correct) using the NATGRID natural-neighbour interpolation library,[2] assuming the best-fitting temperature to lie at the centroid of each bin. The temperatures are emission-weighted, and not corrected for the effects of projection.

In order to demonstrate how the temperature of the cluster changes over its core, we show in Fig. 7 (opposite p. L52) an intensity image of the cluster between 0.3 and 7 keV colour-coded using a temperature map. The temperature map was generated by fitting spectra to bins containing 10^4 counts between 0.5 and 7 keV using the same procedure as above (temperatures accurate from 2 to 4 per cent). The lower temperature regions are coded red, rising through green, to the hotter blue regions (which are hard to see as the brightness of the object drops dramatically to the outer parts of the image).

3 DISCUSSION

The swirl seen in the gross temperature structure is probably due to some angular momentum remaining from the merger history of the Perseus cluster (Fabian et al. 2000; Churazov et al. 2003; Motl et al. 2003). Otherwise, apart from the ripples discussed below, the gas distribution beyond the obvious bubbles (two inner and two outer) and their rims appears to be very smooth. No further bubbles are seen. The bubbles, discussed by Böhringer et al. (1993), Churazov et al. (2000) and Fabian et al. (2000, 2002a), are inflated by the north–south radio jets from the nucleus of NGC 1275. When large enough they detach and rise buoyantly in the intracluster medium.

The ripples seen in the unsharp-masked image (Fig. 3) are intriguing. They appear to be quasi-spherical. A prominent inner one to the north-east, immediately outside the northern bubble, has a sharpish edge. The surface brightness drops by about 20–30 per cent at its edge (Fig. 4). No obvious temperature or abundance changes occur at this point, so it is best explained as a density and pressure change. The amplitude of the first ripple outside the north-west hole, which is about 50 per cent further out than the north-east one, is much smaller at about 10 per cent (Fig. 4), and quantifying the other ripples is difficult.

[1] http://cxc.harvard.edu/cal/Links/Acis/acis/Cal_prods/qeDeg/

[2] http://ngwww.ucar.edu/ngdoc/ng/ngmath/natgrid/nnhome.html

If the ripples are pressure (sound) waves moving at constant speed (about 1170 km s^{-1} for a temperature of 5 keV) then their separation (wavelength) of about 11 kpc means a period of about 9.6×10^6 yr. If the power is constant, the energy flux $\propto \delta P^2/n$, where P and n are the gas pressure and density respectively, should drop with increasing radius r as r^{-2}. Since the density of the intracluster medium drops approximately as r^{-1} in this region (Fabian et al. 2000) then $\delta P/P$ should vary as $r^{-1/2}$ and the relative amplitude of ripples as r^{-1} (since the emissivity mainly depends on the density squared). The observed ripples appear to drop off faster than this, but a much deeper observation is required to confirm it.

The ripples or sound waves may disperse energy throughout the cooling region, which is one important criterion for a successful heat source with which to balance radiative cooling (Fabian 2001; Johnstone et al. 2002). An important issue is whether they dissipate energy throughout this region or not. We have previously assumed that they do not (Fabian et al. 2000). Begelman (2001) and Ruszkowski & Begelman (2002) assume that sound waves and small rising bubbles dissipate their energy on a pressure scalelength in their effervescent model for heating, but give no details of the mechanism. Churazov et al. (2002) argue that rising bubbles are responsible for most of the heating.

First we note that ion viscosity can lead to dissipation of the sound energy within the core. Taking the simple formula of Lamb (1879, also Landau & Lifshitz 1959), the distance L over which the energy of a plane sound wave is reduced by 1/e is given by

$$\frac{L}{\lambda} = \frac{3}{16\pi^2}\frac{c\lambda}{\nu} \sim 7\lambda_{10} n_{0.03} T_5^{-2},$$

where the wavelength $\lambda = 10\lambda_{10}$ kpc, the sound speed is c and viscosity is taken to be $\nu \sim 10^8 T^{5/2} n^{-1}$ cm^2 s^{-1} (Braginskii 1958; Spitzer 1962). The ion density $n = 0.03 n_{0.03}$ cm^{-3} and temperature $T = 5\ T_5$ keV. Thus if the apparent wavelength of about 10 kpc is maintained then the waves dissipate much of their energy within the inner 100 kpc of the cooling region. The viscosity assumed here is high and may of course be significantly affected by magnetic fields in the gas, so the above estimate is uncertain. The Hα filaments around NGC 1275 do, however, provide evidence that the effective Reynolds number is low and therefore that the viscosity is high (Fabian et al. 2003).

Heating will also result from the initial high amplitude of the sound waves, which makes them develop rapidly into weak shocks. The sound speed of the compressed gas is higher [by $(1/3)\delta P/P$] than that in the rarified part, so the wave will steepen in a few wavelengths. The sharp edge or front to the north-east ripple (Figs 1, 4 and 7) indicates that this disturbance is already a weak shock.

In order to study the north-east front in detail we have looked carefully at the density profile in this direction. The density jump across the edge is best determined from a straight surface-brightness deprojection (e.g. Fabian et al. 1981) and is shown in Fig. 8. The ratio of densities at the edge (inner/outer) is $1.43^{+0.20}_{-0.13}$. The projected temperature map (Fig. 6) shows no marked temperature change in this region, although there are a few wisps of cooler gas (red in Fig. 6). There is therefore a large pressure increase going inward over the front and it is not a simple 'cold front' (Markevitch et al. 2000); the inner region is at a higher pressure and the front must be expanding. This is the condition for a weak shock to form. Given the above density jump, continuity over the shock front implies that the temperature should jump by 28 per cent to about $5.8^{+0.8}_{-0.4}$ keV.

To see whether the temperature does jump by this amount, we have deprojected the spectra from five radial zones within a sector across the front. Assuming a single temperature component within each zone, we find that the temperature rises from 3.64 ± 0.08 to 3.90 ± 0.07 keV going inward across the edge. This is partially consistent with a weak shock, which should heat the gas. However, the amplitude of the temperature rise is not as large as expected, and this may be a consequence of the gas being multiphase or initially cooler.

The sharp increase in density combined with the temperature measurements does mean that the inner region is at a higher pressure and should expand outward. The Mach number is 1.5 and the pressure increases by 84 per cent across the shock.

We note that the edge at the shock front is not perfectly sharp; the surface brightness decreases over about 5 arcsec or nearly 2 kpc (we estimate that up to half of this could be due to the point-spread function of the telescope at this off-axis location). This may indicate that the mean-free path, ℓ, is of that order, meaning that the gas is viscous (if $\nu = \frac{1}{3}\ell c$). The front is also seen to the south-west in Fig. 1, and shocked gas probably accounts for all the thick surround to the inner bubbles seen in the hardest image (lower panel of Fig. 2). Projection effects and the multicomponent nature of the emission preclude making any useful spectral analysis of the hotter component.

The above discussion assumes purely hydrodynamical processes. Magnetic fields and cosmic rays in the intracluster gas will complicate many issues, introducing several more wave modes and also tapping the shock energy (which could also contribute to the lack of an observed temperature jump). Particle acceleration will also contribute to the mini-halo radio source (Gitti, Brunetti & Setti 2002).

The rate of work is similar to that required to balance cooling if the bubbles are formed continuously over a Gyr or more at a mean rate of one per 10^7 yr, i.e. the rate deduced from the ripple separation. If we assume that most of the $P\,\mathrm{d}V$ work done on the surrounding gas in inflating each bubble propagates as a sound wave, then the $P\,\mathrm{d}V$ energy of about 270 bubbles, each of 7-kpc radius, is needed to replace the energy radiated by the inner 50 kpc of the cluster, at which radius the radiative cooling time is $\sim 2 \times 10^9$ yr. (A factor of 2 drop in pressure from 12 to 50 kpc is included in this estimate.) It takes 2.5×10^9 yr to produce this number of bubbles if the production rate is on average the same as now. Therefore the rate of bubble production determined from the separation/wavelength of the ripples is close to that required within 50 kpc in order to balance heating and cooling, provided that most of the sound energy is dissipated within that radius by strong viscosity and weak shocks. The bubbles, with the relativistic particles and magnetic fields contained within them, are assumed to rise beyond this region rapidly and become undetectable.

An important problem raised by the heating mechanism proposed here is the significant rims of cool gas around the bubbles. They may, however, just be a collection of cooler blobs which have been swept up and not shocked (Fabian et al. 2001). Such blobs may be magnetically uncoupled from the hotter phase, and therefore not conductively evaporated, and are on a scale which is much smaller than the wavelength of the sound waves. This means that any pressure differences caused by these waves across the blobs vary more slowly than the internal sound crossing time and no shock occurs.

In summary, the deep *Chandra* observation of the Perseus cluster has revealed subtle ripples, which could be the sound waves that transport and dissipate the energy of the bubbles which continuously form at the centre. The process is due not to effervescence of many small bubbles (Begelman 2001), to rare major eruptions (Soker et al. 2001; Kaiser & Binney 2002) or to the buoyant bubbles themselves (Churazov et al. 2001), but to a more continuous dissipation of acoustic energy as the (attached) bubbles grow. More study is needed

to determine whether further heating is required at larger radii and whether this process can account for the heating in more luminous objects which (currently) do not have any major central radio source [e.g. A1835 (Fabian et al. 2002b); sound waves, generated in the outer hot gas by subcluster mergers, are refracted inward (Pringle 1989) by the denser core gas, and may provide the explanation here]. The much-sought detailed connection between the active nucleus, which is possibly fuelled by the hot surrounding gas, and the required distributed heat source in the inner intracluster medium has come to light in the Perseus cluster.

ACKNOWLEDGMENTS

We thank the referee and Jeremy Goodman for helpful comments, and the *Chandra Observatory* team for such superb data. ACF, SWA and CSC thank the Royal Society for support.

REFERENCES

Anders E., Grevesse N., 1989, Geochim. Cosmochim. Acta, 53, 197
Balucinska-Church M., McCammon D., 1992, ApJ, 400, 699
Basson J. F., Alexander P., 2003, MNRAS, 339, 353
Begelman M. C., 2001, in Hibbard J. E., Rupen M. P., van Gorkom J. H., eds, ASP Conf. Ser. Vol. 240, Gas & Galaxy Evolution. Astron. Soc. Pac., San Francisco, p. 363
Bertschinger E., Meiksin A., 1986, ApJ, 306, L1
Böhringer H., Voges W., Fabian A. C., Edge A. C., Neumann D. M., 1993, MNRAS, 264, L25
Böhringer H., Matsushita K., Churazov E., Ikebe Y., Chen Y., 2002, A&A, 382, 804
Braginskii S. L., 1958, Sov. Phys. JETP, 6, 358
Brighenti F., Mathews W. G., 2003, ApJ, 587, 580
Brüggen M., Kaiser C. R., 2001, MNRAS, 325, 676
Cappellari M., Copin Y., 2003, MNRAS, 342, 345
Chartas G., Getman K., 2002, http://www.astro.psu.edu/users/chartas/xcontdir/xcont.html
Churazov E., Forman W., Jones C., Böhringer H., 2000, A&A, 356, 788
Churazov E., Brüggen M., Kaiser C. R., Böhringer H., Forman W., 2001, ApJ, 554, 261
Churazov E., Sunyaev R., Forman W., Böhringer H., 2002, MNRAS, 332, 729
Churazov E., Forman W., Jones C., Böhringer H., 2003, ApJ, 590, 225
Conselice C. J., Gallagher J. S., Wyse R. F. G., 2001, AJ, 122, 2281
Fabian A. C., 1994, ARA&A, 32, 277
Fabian A. C., 2001, in Laing R. A., Blundell K. M., eds, ASP Conf. Ser. Vol. 250, Particles and Fields in Radio Galaxies. Astron. Soc. Pac., San Francisco, p. 471
Fabian A. C., Hu E. M., Cowie L. L., Grindlay J., 1981, ApJ, 248, 47
Fabian A. C. et al., 2000, MNRAS, 318, L65
Fabian A. C., Mushotzky R. F., Nulsen P. E. J., Peterson J. R., 2001, MNRAS, 321, L20
Fabian A. C., Celotti A., Blundell K. M., Kassim N. E., Perley R. A., 2002a, MNRAS, 331, 369
Fabian A. C., Allen S. W., Crawford C. S., Johnstone R. M., Morris R. G., Sanders J. S., Schmidt R. W., 2002b, MNRAS, 332, L50
Fabian A. C., Voigt L. M., Morris R. G., 2002, MNRAS, 335, L71
Fabian A. C., Sanders J. S., Crawford C. S., Conselice C. J., Gallagher J. S., III, Wyse R. F. G., 2003, MNRAS, 344, L48 (this issue)
Gitti M., Brunetti G., Setti G., 2002, A&A, 386, 456
Johnstone R. M., Allen S. W., Fabian A. C., Sanders J. S., 2002, MNRAS, 336, 299
Kaiser C. R., Binney J., 2002, MNRAS, 338, 837
Lamb H., 1879, Hydrodynamics. Cambridge Univ. Press, Cambridge
Landau L. D., Lifshitz E. M., 1959, Fluid Dynamics. Pergamon Press, Oxford
Liedahl D. A., Osterheld A. L., Goldstein W. H., 1995, ApJ, 438, L115
Lynds R., 1970, ApJ, 159, L151
Markevitch M. et al., 2000, ApJ, 541, 542
Mewe R., Gronenschild E. H. B. M., van den Oord G. H. J., 1985, A&AS, 62, 197
Morris R. G., Fabian A. C., 2003, MNRAS, 338, 824
Motl P. M., Burns J. O., Loken C., Norman M. L., Bryan G., 2003, ApJ, in press (astro-ph/0302427)
Narayan R., Medvedev M. V., 2001, ApJ, 562, L129
Pedlar A., Ghataure H. S., Davies R. D., Harrison B. A., Perley R., Crane P. C., Unger S. W., 1990, MNRAS, 246, 477
Peterson J. et al., 2001, A&A, 365, L104
Peterson J. R., Kahn S. M., Paerels F. B. S., Kaastra J. S., Tamura T., Bleeker J. A. M., Farrigno C., Jernigan J. G., 2003, ApJ, 590, 207
Pringle J. E., 1989, MNRAS, 239, 474
Quilis V., Bower R. G., Balogh M. L., 2001, MNRAS, 328, 1091
Reynolds C. S., Heinz S., Begelman M. C., 2001, ApJ, 549, L179
Ruszkowski M., Begelman M. C., 2002, ApJ, 581, 223
Schmidt R. W., Fabian A. C., Sanders J. S., 2002, MNRAS, 337, 71
Soker N., White R. E., David L. P., McNamara B. R., 2001, ApJ, 549, 832
Spitzer L., 1962, The Physics of Fully Ionized Gases. Interscience Publishers, New York
Tabor G., Binney J., 1993, MNRAS, 263, 323
Tamura T. et al., 2001, A&A, 365, L87
Tucker W., Rosner R., 1983, ApJ, 267, 547
Voigt L. M., Schmidt R. W., Fabian A. C., Allen S. W., Johnstone R. M., 2002, MNRAS, 335, L7
Zakamska N. L., Narayan R., 2003, ApJ, 582, 162

This paper has been typeset from a TEX/LATEX file prepared by the author.

Opposite p. L52, MNRAS, **344**

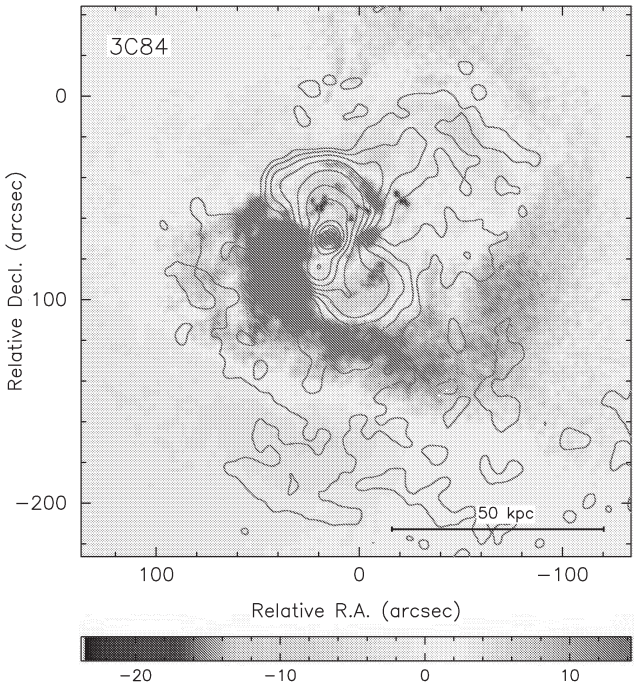

Figure 5. Deprojected 0.3–7 keV X-ray image, convolved by a 0.98-arcsec Gaussian, overlaid with contours from the 328-MHz VLA image at a resolution of 8 arcsec. Contours are drawn at 0.011, 0.022, . . . , and 5.63 Jy beam^{-1}. The peak in the radio image is 8.78 Jy beam^{-1} and the noise is 0.0016 Jy beam^{-1}. In addition to filling the inner X-ray cavities, one can also see a spur of radio emission extending into the X-ray hole to the north-west.

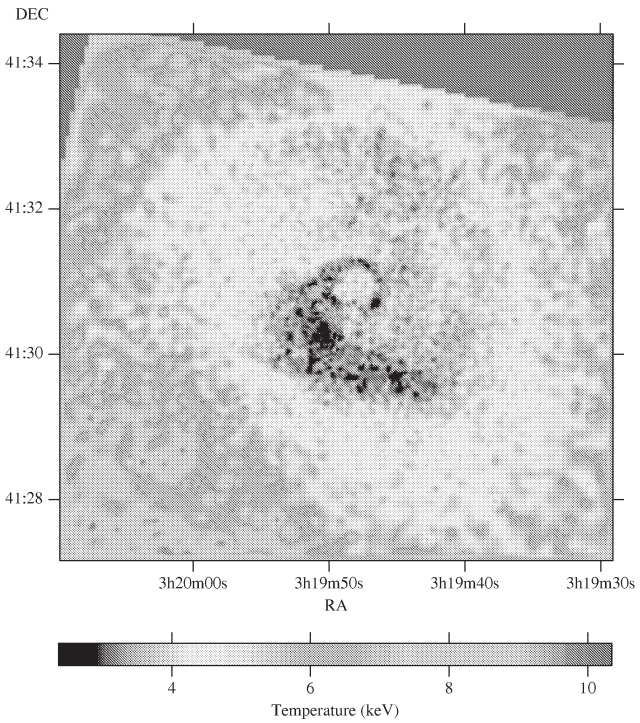

Figure 6. Smoothed temperature map, from spectra in bins with 2000 counts.

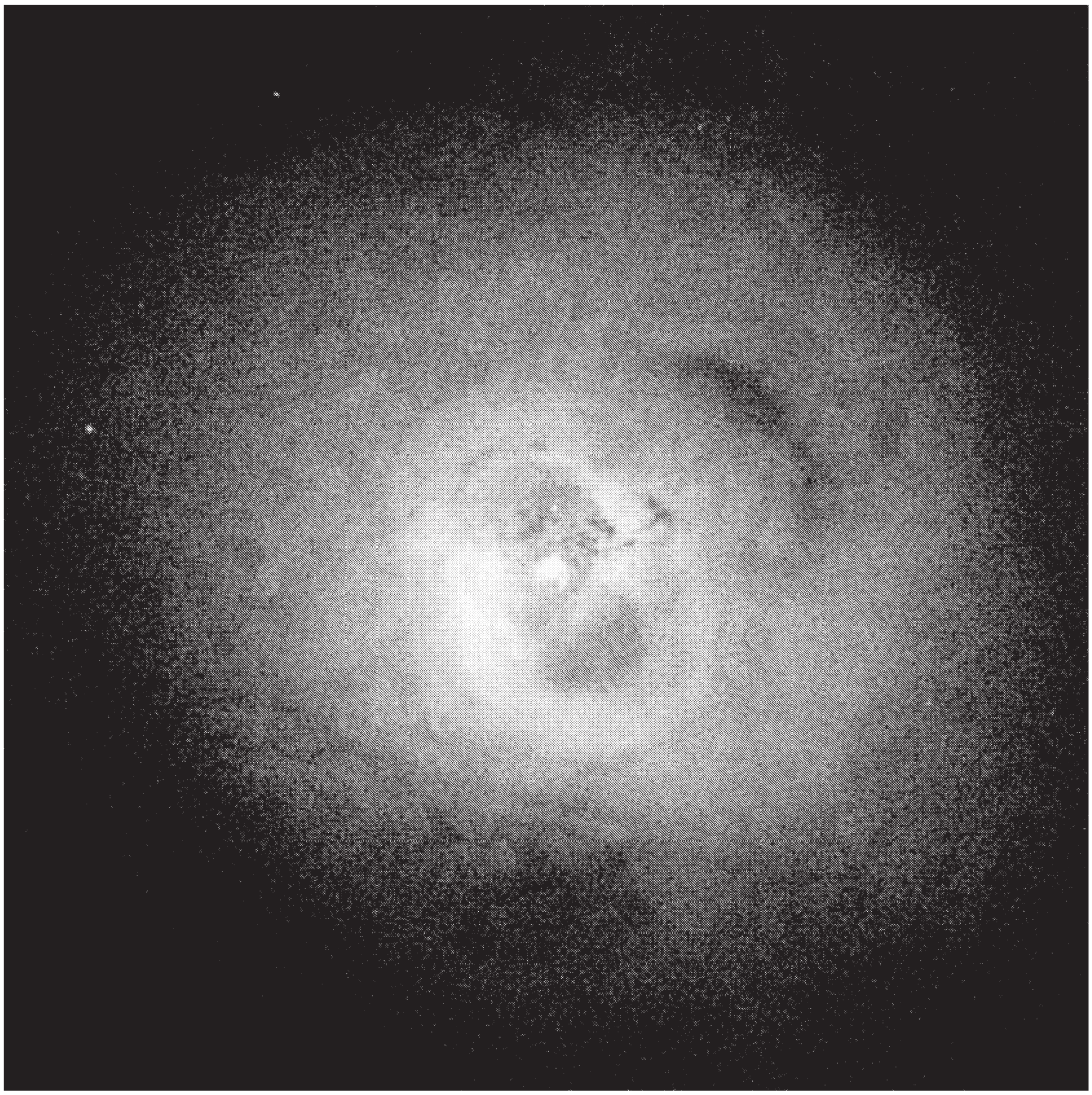

Figure 7. X-ray intensity between 0.3 and 7 keV, colour-coded by temperature (see Section 2). The image is 350 arcsec (131 kpc) square.